



Deposited via The University of Sheffield.

White Rose Research Online URL for this paper:

<https://eprints.whiterose.ac.uk/id/eprint/163220/>

Version: Accepted Version

Article:

Verbruggen, S.W., Mc Garrigle, M.J., Haugh, M.G. et al. (2015) Altered mechanical environment of bone cells in an animal model of short- and long-term osteoporosis. *Biophysical Journal*, 108 (7). pp. 1587-1598. ISSN: 0006-3495

<https://doi.org/10.1016/j.bpj.2015.02.031>

Article available under the terms of the CC-BY-NC-ND licence
(<https://creativecommons.org/licenses/by-nc-nd/4.0/>).

Reuse

This article is distributed under the terms of the Creative Commons Attribution-NonCommercial-NoDerivs (CC BY-NC-ND) licence. This licence only allows you to download this work and share it with others as long as you credit the authors, but you can't change the article in any way or use it commercially. More information and the full terms of the licence here: <https://creativecommons.org/licenses/>

Takedown

If you consider content in White Rose Research Online to be in breach of UK law, please notify us by emailing eprints@whiterose.ac.uk including the URL of the record and the reason for the withdrawal request.

1 **The micromechanical environment of osteoblasts and osteocytes is altered in an animal**
2 **model of short- and long-term osteoporosis**

3 S.W. Verbruggen, M.J. Mc Garrigle, M.G. Haugh, M.C. Voisin,

4 L.M. McNamara*

5 Biomechanics Research Centre (BMEC),

6 National Centre for Biomedical Engineering Science (NCBES),

7 Biomedical Engineering, College of Engineering and Informatics,

8 National University of Ireland, Galway

9
10 Address for correspondence:

11 Dr. Laoise M. McNamara

12 Department of Mechanical and Biomedical Engineering

13 National University of Ireland Galway

14 Galway,

15 Ireland

16 Phone: (353) 91-492251

17 Fax: (353) 91-563991

18 Email: Laoise.McNamara@nuigalway.ie

19 Running Title: In vivo loading of bone cells during osteoporosis

20 Key words of the paper: Bone, osteocyte, osteoblast, mechanobiology, mechanical loading, strain

1
2
3
4
5
6
7
8
9
10
11
12
13
14
15
16
17
18
19
20
21
22
23
24
25

ABSTRACT

Alterations in bone tissue composition during osteoporosis likely disrupt the mechanical environment of bone cells and may thereby initiate a mechanobiological response. It has proved challenging to characterise the mechanical environment of bone cells *in vivo*, and the mechanical environment of osteoporotic bone cells is not known. The objective of this research is to characterise the local mechanical environment of osteocytes and osteoblasts from healthy and osteoporotic bone in a rat model of osteoporosis. Using a custom-designed micromechanical loading device, we apply strains representative of a range of physical activity (up to 3,000 $\mu\epsilon$) to fluorescently stained femur samples from normal and ovariectomised rats. Confocal imaging was simultaneously performed, and digital image correlation techniques were applied to characterise cellular strains. In healthy bone tissue osteocytes experience higher maximum strains ($31,028 \pm 4,213 \mu\epsilon$) than osteoblasts ($24,921 \pm 3,832 \mu\epsilon$), whereas a larger proportion of the osteoblast experiences strains above 10,000 $\mu\epsilon$. Most interestingly, we show that osteoporotic bone cells experience similar or higher maximum strains than healthy bone cells after short durations of oestrogen deficiency (5 weeks), and exceeded the osteogenic strain threshold (10,000 $\mu\epsilon$) in a similar or significantly larger proportion of the cell (osteoblast: 12.68% vs. 13.68%; osteocyte: 15.74% vs. 5.37%). However, in long-term oestrogen deficiency (34 weeks) there was no significant difference between bone cells in healthy and osteoporotic bone. These results suggest that the mechanical environment of bone cells is altered during early-stage osteoporosis, and that mechanobiological responses act to restore the mechanical environment of the bone tissue after it has been perturbed by ovariectomy.

1. INTRODUCTION

The interconnected network of osteocytes and osteoblasts in bone tissue is believed to act as the driving force behind bone adaptation, allowing bone tissue to actively remodel its mass and structure in response to the mechanical demands experienced throughout life. Osteocytes and osteoblasts are known to be mechanosensitive, recruiting osteoblasts and osteoclasts to orchestrate an adaptive response when the mechanical environment is not favourable (1-6).

Osteoporosis is a debilitating bone disease, which is characterised by an imbalance in normal bone cell remodelling (7), and results in severe bone loss (8), significantly reduced strength (9, 10) and altered bone tissue porosities (11-13). Previous studies have shown altered mechanical properties of trabecular bone in ovariectomized rats compared to sham-operated controls (14, 15). Furthermore, tissue-level mineral distribution is altered in a sheep model of osteoporosis (16), and changes in mineralized crystal maturity, mineral-to-matrix ratio, and collagen cross-linking also occur (10). Such changes might occur as a compensatory mechanism triggered by bone loss during osteoporosis. Alternatively, it may be that oestrogen deficiency itself leads directly to changes in tissue composition, which consequently alters the local mechanical environment of osteoblasts and osteocytes. This change in mechanical stimuli sensed by bone cells may then initiate a mechanoregulatory response resulting in bone loss. Computational simulations of bone adaptation have predicted osteoporotic-like trabecular architecture (17), and altered bone resorption rates and osteocyte strain levels (18) in response to changes in tissue stiffness. However, it remains that the mechanical stimulation experienced by bone cells within osteoporotic bone in vivo has never been characterised and, as such, these theories remain conjecture.

As osteocytes are embedded in a mineralized matrix, direct experimental investigation of their mechanical environment is challenging. High resolution microscopy of exposed two-dimensional bone sections under mechanical loading (19) have predicted perilacunar strains in the range of 7,500-35,000 $\mu\epsilon$ (20, 21). AFM techniques have measured osteoblast strains as high as 40,000 $\mu\epsilon$ under an applied load of 20 nN in vitro (22, 23). These high strain levels are significant, as previous in vitro cell culture studies have observed an osteogenic response in osteoblastic cells at magnitudes greater than a threshold of approximately 10,000 $\mu\epsilon$ (6, 24). However, the experimental approaches of Nicolella et al. involved milled sections of bone tissue and surface polishing to expose embedded osteocytes (20, 21), and such methods might alter the mechanical environment of the cell (25, 26). Furthermore, point loading through AFM techniques is not representative of the substrate strain that osteoblasts on bone surfaces are exposed to in vivo. Computational modelling of the in vivo strain environment of individual osteocytes has predicted strains of 23-26,000 $\mu\epsilon$ occurring in the osteocyte for an applied load of 3,000 $\mu\epsilon$ (27), whereas osteoblasts were shown to experience maximum strains of approximately 1,270 $\mu\epsilon$ for applied loading of 1,000 $\mu\epsilon$ (22, 23). While these models provide an insight into bone cell mechanical behaviour, an experimental approach, which does not necessitate destruction of or interference with the local mechanical environment, is required to investigate the in situ strain environment of cells in healthy and osteoporotic bone.

Confocal microscopy has been widely applied to visualise the lacunar-canalicular network (28-31), osteocytes (32-36), and microcracking within bone tissue (25, 26). Confocal

1 microscopy techniques have been recently combined with in situ mechanical loading to
2 investigate cell mechanics within the intervertebral annulus fibrosus (37) and cartilage under
3 loading (38). However, such methods have never been applied to characterise the local
4 mechanical environment of bone cells in vivo.

5 The objective of this research is to characterise the local mechanical environment of
6 osteocytes and osteoblasts from normal and osteoporotic bone in a rat model of osteoporosis.
7 We design a purpose-built micromechanical loading rig, and combined this with a confocal
8 microscopy and DIC imaging technique, to characterise the mechanical environment of
9 osteoblasts and osteocytes in situ under physiological loading conditions. We investigate the
10 local mechanical environments of osteocytes and osteoblasts after 5 and 34 weeks oestrogen
11 deficiency, and compare these to cells within the bone tissue of sham operated controls.

12

13 **2. MATERIALS AND METHODS**

14 **2.1. Custom-designed loading device**

15 In order to visualise the local mechanical environment of the cells, a custom loading device
16 was designed that is compatible with a confocal microscope (Zeiss LSM 51) and comprised a
17 specialised loading stage and sample grips to ensure that samples could be held flush with the
18 microscope objective (Fig. 1). A high-torque stepper motor (ST2818L1006, Nanotec) and
19 gearing provided transmission to a precision bi-directional ball power screw (SD0401,
20 ABSSAC), and thus applied micro-scale displacements to cortical bone samples (of length 10
21 mm) during imaging. The applied loading is displacement-controlled, with displacements
22 applied to the whole bone in specified increments, with speeds and magnitudes controlled
23 using commercial software (NanoPro 1.6, Nanotec). The device is capable of applying bi-
24 directional uniaxial tensile or compressive loading at increments as small as 50 $\mu\epsilon$.

25

26

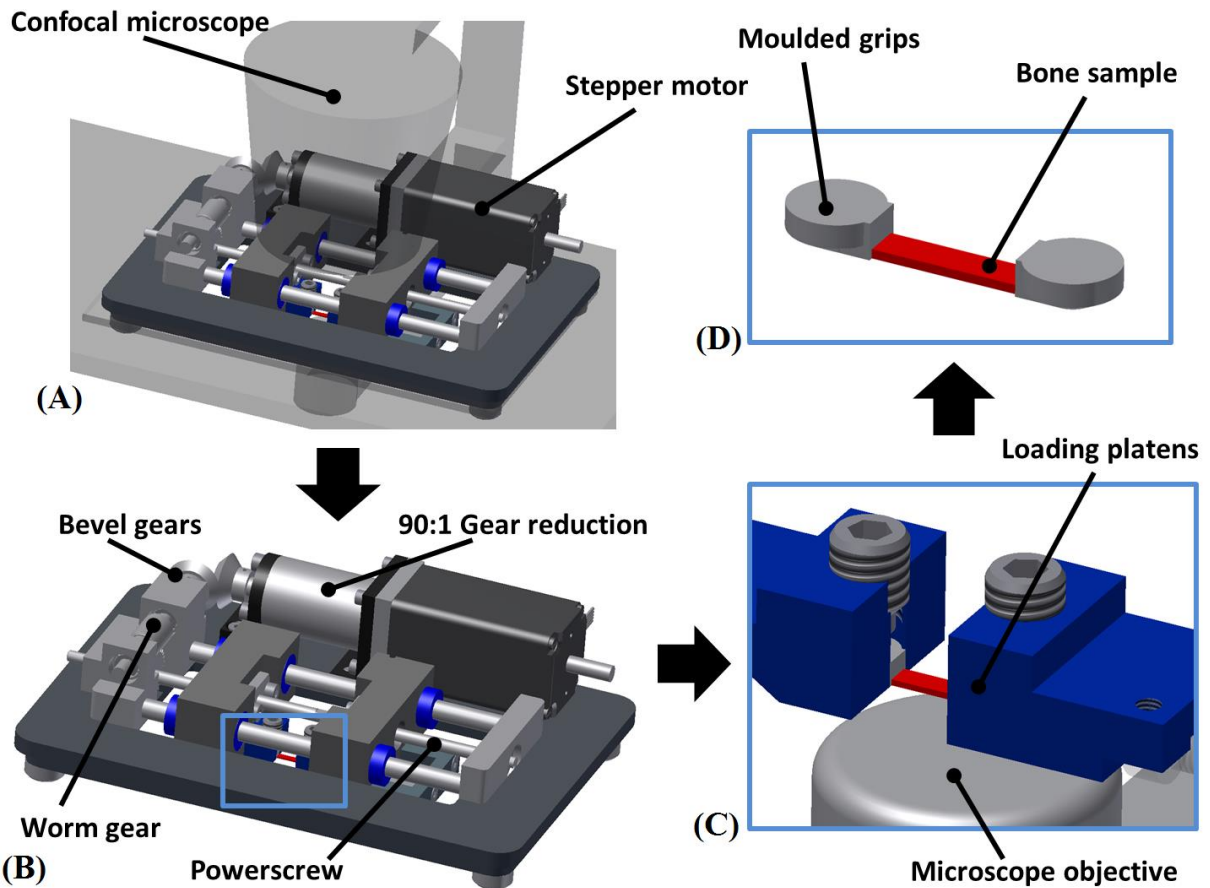


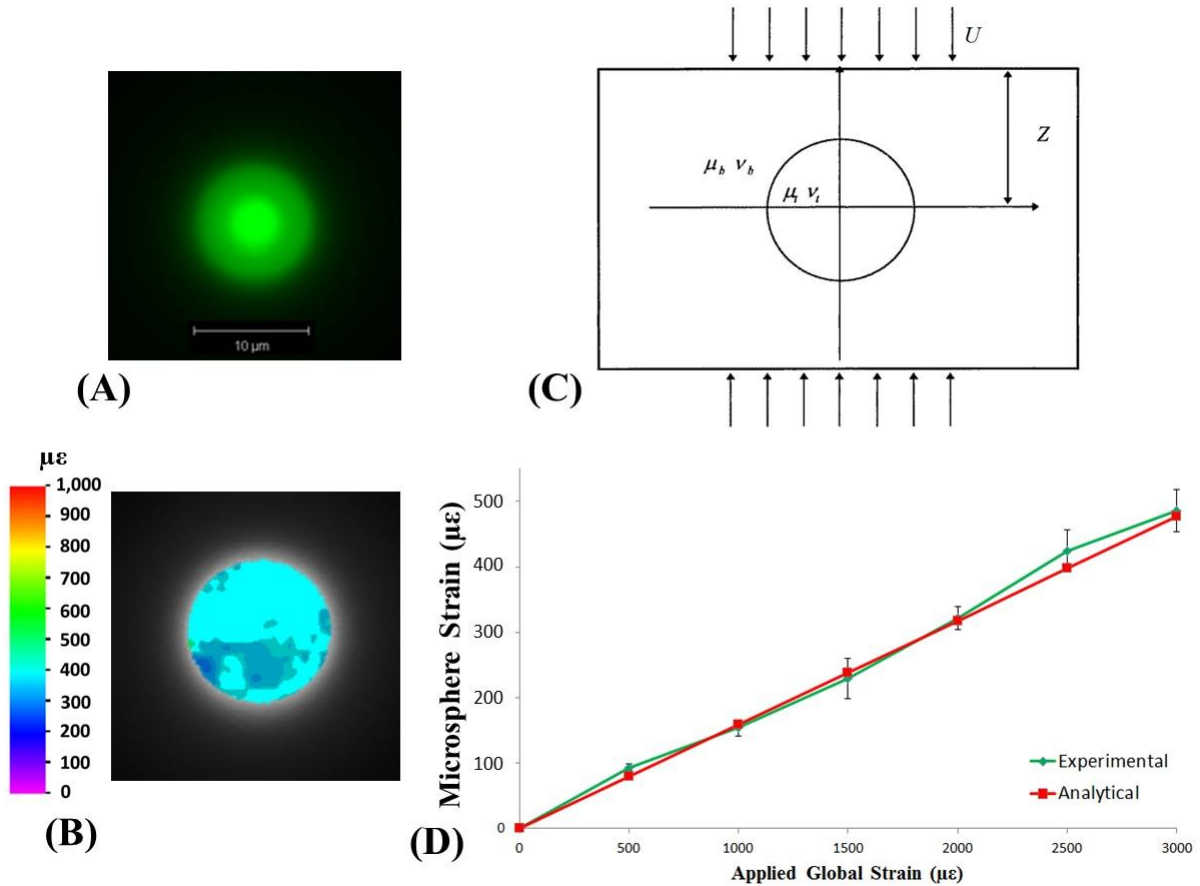
FIGURE 1: Diagram of custom-designed micro-loading device in position under the confocal microscope (A) and close-up (B). Relationship between bone sample, loading platens and microscope objective shown in (C) and (D).

2.2. Validation of loading device and DIC analysis

The custom-built loading device was validated for the application of bi-directional, uniaxial compression loading on a poly(methyl methacrylate) (PMMA) sample (length 12 mm and radius 3.2 mm) with embedded fluorescent microspheres. Briefly, a PMMA resin (8510, Akasol), was combined with a curing agent (8562, Akasol) and fluorescent microspheres (10 μm diameter) at a dilution of 1 $\mu\text{L}/\text{mL}$ (Fluoresbrite 18140-2, Polysciences Inc.). A sonicator (2510E-MT, Branson Ultrasonics) and rotator (SB3, Stuart) were used to ensure dispersion of the microspheres throughout the sample. The samples were formed by filling 12 mm lengths of 3.2 mm diameter silicone tubing (HV-96410-16, Masterflex) with the PMMA resin and allowing it to set overnight. The cylindrical samples were then extracted from the tubing and inserted into the grips for the experimental loading.

A compressive displacement load equivalent to 3,000 μe was applied to the PMMA/microsphere construct and a series of confocal images were captured for Digital Image Correlation (DIC) analysis (see Fig. 2A). The strain distribution within each sphere was determined from a series of images of each loaded sphere using DIC analysis with a previously developed software package (MOIRE) (39-41), which is capable of tracking displacements of pixels in the images (see Fig. 2B). A correlation coefficient is calculated for

1 each pixel by comparing the deformed image with the reference image. A zero-mean
 2 normalised cross-correlation (ZNCC) coefficient is then determined for each image pixel.
 3 Once the correlation coefficient extremes (maximum and minimum) have been detected, the
 4 full-field deformation can be determined, providing a measure of the maximum principal
 5 strain. The loading and DIC analysis was repeated for ten different microspheres and
 6 compared to the results of an analytical solution for a homogenous material with spherical
 7 inclusions under loading (42).



8

9 **FIGURE 2: Confocal image of PMMA-embedded fluorescent microsphere (A), with the**
 10 **contour plot of strain within it under 3,000 $\mu\epsilon$ loading (B). Diagram of analytical**
 11 **solution for spherical inclusion in an homogenous material (C), adapted from (42).**
 12 **Comparison of experimental and analytical results over a range of applied loads is**
 13 **shown in (D).**

14

15 Briefly, the analytical solution allows for calculation of the strain within a spherical object
 16 embedded in a homogenous material of different material properties (see Fig. 2C). The
 17 relationship between the strain, material properties, geometry and displacement is
 18 summarised in the following equation:

$$e = \left(\frac{U}{Z}\right) \left(\frac{2\mu_b(1 + \nu_b)(1 - \nu_b)}{2(1 + \nu_b)} \right) \left(- \frac{5(1 - \nu_b)}{[\mu_b(7 - 5\nu_b) + \mu_t(8 - 10\nu_b)]} + \frac{(1 - 2\nu_t)}{[\mu_b(2 - 4\nu_t) + \mu_t(1 + \nu_t)]} \right)$$

1 where the shear modulus and Poisson's ratio are denoted by μ_b , ν_b and μ_t , ν_t for the matrix
 2 and microsphere respectively, strain is denoted by e , displacement by U and specimen length
 3 by $2Z$ (42). PMMA was assumed to have a shear modulus of 1.7 GPa and Poisson's ratio of
 4 0.3, while values of 2.1 MPa and 0.3 were assumed for the polystyrene microspheres.

5 Analysis of the experimental results was compared to the analytical solution at load steps of
 6 500 $\mu\epsilon$, 1,000 $\mu\epsilon$, 1,500 $\mu\epsilon$, 2,000 $\mu\epsilon$ and 2,500 $\mu\epsilon$ and 3,000 $\mu\epsilon$. The strain observed
 7 experimentally displayed close correlation to the analytical solution over multiple applied
 8 loads, see Fig. 2D. The percentage error at each of the 500 $\mu\epsilon$, 1,000 $\mu\epsilon$, 1,500 $\mu\epsilon$, 2,000 $\mu\epsilon$,
 9 2,500 $\mu\epsilon$ and 3,000 $\mu\epsilon$ load steps was 9.41%, 3.37%, 4.13%, 1.14%, 6.81% and 1.88%
 10 respectively. At 3,000 $\mu\epsilon$ an average strain within the microspheres of 486 $\mu\epsilon$ ($486 \pm 32.1 \mu\epsilon$)
 11 was observed by the DIC technique, while the analytical solution predicts a value of 477 $\mu\epsilon$.

12 2.3. Animal Model and Sample Preparation

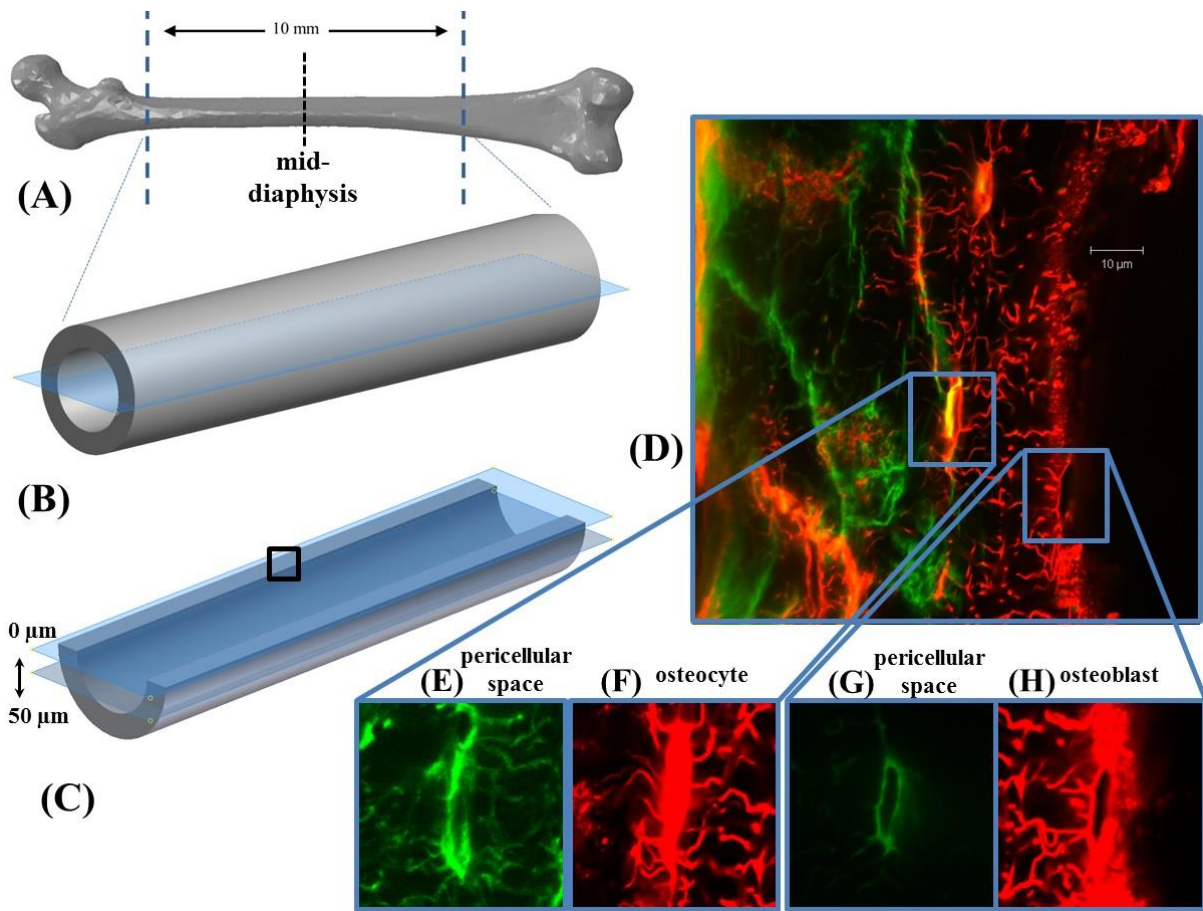
13 Ovariectomised rat bone is employed in this study as it has been deemed an appropriate
 14 model for post-menopausal osteoporosis in humans (43), with many shared characteristics
 15 with human diseased bone (44). Four groups of 8-month old female Wistar (Charles River)
 16 rats were used in this study; (1) a group in which rats were ovariectomised five weeks prior to
 17 the experiment (n=4) to induce oestrogen deficiency, (2) a control sham-operated group
 18 (n=4), and a 34-week postoperative (3) ovariectomised (n=2) and (4) control sham group
 19 (n=2). Animals were anaesthetised using isoflurane gas and then sacrificed by CO₂
 20 inhalation. Upon sacrifice of the animals, checks were performed to confirm the presence or
 21 absence of the ovaries for SHAM and OVX animals respectively. Immediately prior to
 22 sacrifice, rats were injected with FITC (Fluorescein Isothiocyanate Isomer 1, 30 μL at 10
 23 mg/mL, Sigma-Aldrich F7250) to stain the lacunar-canalicular network, similar to previous
 24 methods (28). All procedures were carried out following institutional ethical approval and
 25 under an animal license granted by the Irish Department of Health B100/4424.

26 One femur from each animal was extracted and placed in α -minimum essential medium
 27 (α -MEM) supplemented with 10% foetal bovine serum (FBS), 2 mM L-glutamine, 100 U/mL
 28 penicillin and 100 $\mu\text{g/mL}$ streptomycin (all Sigma-Aldrich) at 37 °C, in order to maintain cell
 29 viability within the samples. Additionally, the experimental study was performed in less than
 30 five hours to minimise post-extraction time.

31 Femurs extracted from rats were cut proximally and distally using a diamond blade saw
 32 (Isomet, Buehler) to produce 10 mm femoral shaft specimens. These were further cut to
 33 produce longitudinal, semi-cylindrical samples that could be loaded and imaged
 34 simultaneously in our custom device (see Fig. 3(A-C)). The live samples were kept in media
 35 during cutting and preparation, and rinsed with phosphate-buffered saline (PBS) solution

1 immediately prior to loading to prevent auto-fluorescence of the media. After cutting and
 2 prior to loading, samples were incubated for 30 minutes in FITC to enhance staining and a
 3 plasma membrane stain (CellMask Orange Plasma Membrane, 20 μ L at 5 mg/mL, Invitrogen
 4 C10045) in order to visualise the osteoblast and osteocyte cell membranes. All preparation
 5 and loading occurred within five hours after extraction, with samples covered in aluminium
 6 foil to prevent photobleaching. PBS was regularly applied to samples during loading and
 7 imaging to prevent dehydration. Custom-designed epoxy resin grips were made for each
 8 sample using a mould to prevent bone fracture and edge effects during loading.

9
 10



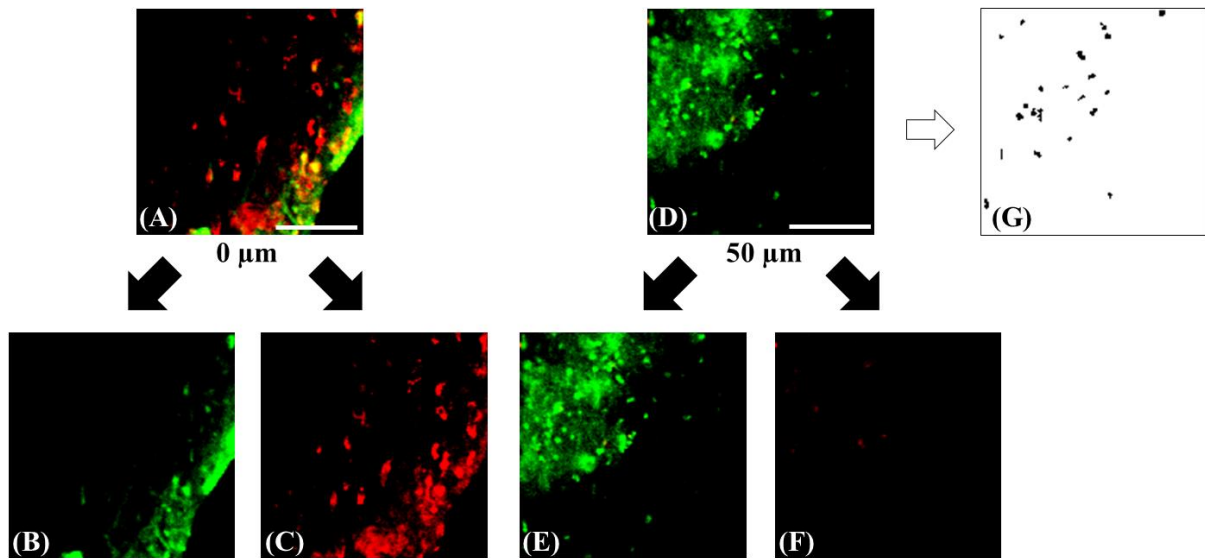
11

12 **FIGURE 3: Diagram of removal of proximal and distal ends of femur, followed by**
 13 **longitudinal sectioning of the sample (A-C). Imaging was performed at the mid-**
 14 **diaphysis, approximately 50 μ m below the cut surface, indicated by the dotted line in**
 15 **(A) and the box in (C). Confocal scans performed from cut face through depth of bone**
 16 **(D), allowing visualisation of the lacunar-canalicular network (E) and osteoblast**
 17 **pericellular space in green (G), and the osteocytes (F) and osteoblasts (H) in red.**

1 **2.4. Confocal Imaging and Mechanical Loading Conditions**

2 Using the custom-built loading device, bi-directional, uniaxial compression loading up to
3 3,000 $\mu\epsilon$, levels at which bone cell stimulation has been predicted experimentally and
4 computationally (27, 45, 46), was applied longitudinally to the bone samples at a strain rate
5 of 83.3 $\mu\epsilon/s$. Bone cells were imaged in the mid-diaphysis of the femur in order to avoid
6 characterising cells that might experience large displacements occurring near the grips.
7 Confocal scans (Zeiss LSM 51) were taken with a 63x oil immersion lens, with 0.08 mm thick
8 glass coverslips (CB00070RA1, Menzel-Glaser) separating the moisture in the sample from
9 immersion oil and allowing imaging through the depth of the sample. Wavelength excitations
10 of 488 nm and 543 nm were applied to scan the pericellular space and the cell membrane
11 respectively (see Fig. 3D), with an image size of 255 x 255 μm . The image frame size was
12 1024 x 1024 pixels, which gives a pixel size (resolution) of 0.1 μm and the optical slice
13 thickness was 0.6 μm . Multi-tracking was also performed to illuminate both the pericellular
14 spaces in green and the osteocyte and osteoblast cells contained within (see Fig. 3E and 3G,
15 and Fig. 3F and 3H, respectively). Confocal scans of the osteocytes and osteoblasts near the
16 periosteal surface can be seen in red in Fig. 3F and 3H respectively. These scans can be
17 analysed separately to elucidate the detail of the lacunar-canalicular space in isolation from
18 the cell, and vice-versa (visible by comparing Fig. 3E and 3F). Only the scans of the
19 individual cells, in red, were investigated in the DIC analysis. Imaging was performed at a
20 depth of at least 50 μm , away from damaged regions from the cutting process. At this depth
21 osteocytes are easily discriminated due to their location within the bone. For simplicity we
22 refer to “osteoblasts”, but indeed these observations also apply to the quiescent bone lining
23 osteoblasts on the surface.

24 Scans were taken of the cells every 3 seconds for each 250 $\mu\epsilon$ loading step in order to build a
25 series of images to represent cell deformation during loading. This process was repeated for
26 each femur sample loaded, allowing imaging of ten osteoblasts and ten osteocytes per
27 specimen. The mechanical behaviour of individual cells was consistent over the course of
28 repeated loading cycles (≤ 10 cycles). This resulted in a total of 240 cells, with 160 and 80 of
29 each cell type for both OVX and SHAM animals, at 5- and 34-weeks post-operation
30 respectively. Sample images of both an osteocyte and osteoblast are shown at 0 $\mu\epsilon$ in Fig. 5A
31 and 4B respectively.



1

2

3

4

5

FIGURE 4: Confocal scans of the same location in a femur sample at (A) 0 μm and (D) 50 μm from the cut surface. Cell viability is indicated by green staining (B and E), while cytotoxicity is denoted by red (C and F) (scale bar: 100 μm). Thresholding of (D) for quantification of cell viability is shown in (G).

6

2.5. Cell Viability

7

8

9

10

11

12

13

14

15

16

17

18

19

20

21

22

In order to investigate whether cells at our chosen imaging plane were affected by the cutting process, a cell viability study was performed. A femur was harvested from a 4-month old female Wistar rat, sectioned and processed as described above. The sample was then incubated in a Live/Dead Viability/Cytotoxicity assay (L-3224, Invitrogen) for three hours. Confocal scans of the sample were taken five hours post-extraction at depths of 0 and 50 μm below the cut surface. These scans were performed at 10x magnification using an excitation wavelength of 488 nm. The resulting images are shown in Fig. 4, with green indicating viability and red indicating cytotoxicity due to ruptured cell membranes. Additionally, thresholding was performed in order to use “island counting” techniques in ImageJ (see Fig. 4G) to quantify the percentage of live and dead cells at each depth: 34.7% live vs. 65.2% dead at 0 μm ; 89% live vs. 11% dead at 50 μm . This demonstrates that although cell death occurs at the cut surface, at a distance 50 μm from the surface (the location at which the strain analyses are conducted) there is a substantial population of live cells (89%). As damage to the surrounding matrix would likely have a detrimental effect on cell viability, we can infer that the local mechanical environment of the osteocyte is not substantially damaged during cutting.

23

2.6. Digital Image Correlation (DIC) Analysis

24

25

26

27

28

The DIC methods described above were applied to analyse a series of images of the loaded osteocytes and osteoblasts, shown at 0 μm in Fig. 5A and 5B respectively. This allowed the strain field in the cells to be calculated, providing contour plots of maximum principal strain distributions within the cells, shown in Fig. 5C and 5D. The percentage area of a cell stimulated within a specific range of strain is determined by dividing the number of pixels at

1 strain values within this range by the total number of pixels that represent the cell. This
2 allowed determination of the percentage area of each cell that exceeds the osteogenic strain
3 threshold, which is taken as 10,000 $\mu\epsilon$ (6, 24). As this is a 2D DIC analysis, the contour plots
4 represent a section through the cell and the strain results are presented as a percentage area of
5 this section of the cell.

6 **2.7. Statistical Analysis**

7 Ten of each bone cell type were analysed from each bone sample, with n=4 animals per
8 group at 5 weeks post-operation (SHAM-5, OVX-5) and n=2 animals per group at 34 weeks
9 post-operation (SHAM-34, OVX-34). All data are expressed as a mean \pm standard deviation.
10 Statistical differences between groups were determined using the non-parametric Kruskal-
11 Wallis method. Dunn's test method for comparison between groups was used to determine
12 statistical significance defined as $p < 0.05$ (MINITAB v. 16).

13

14

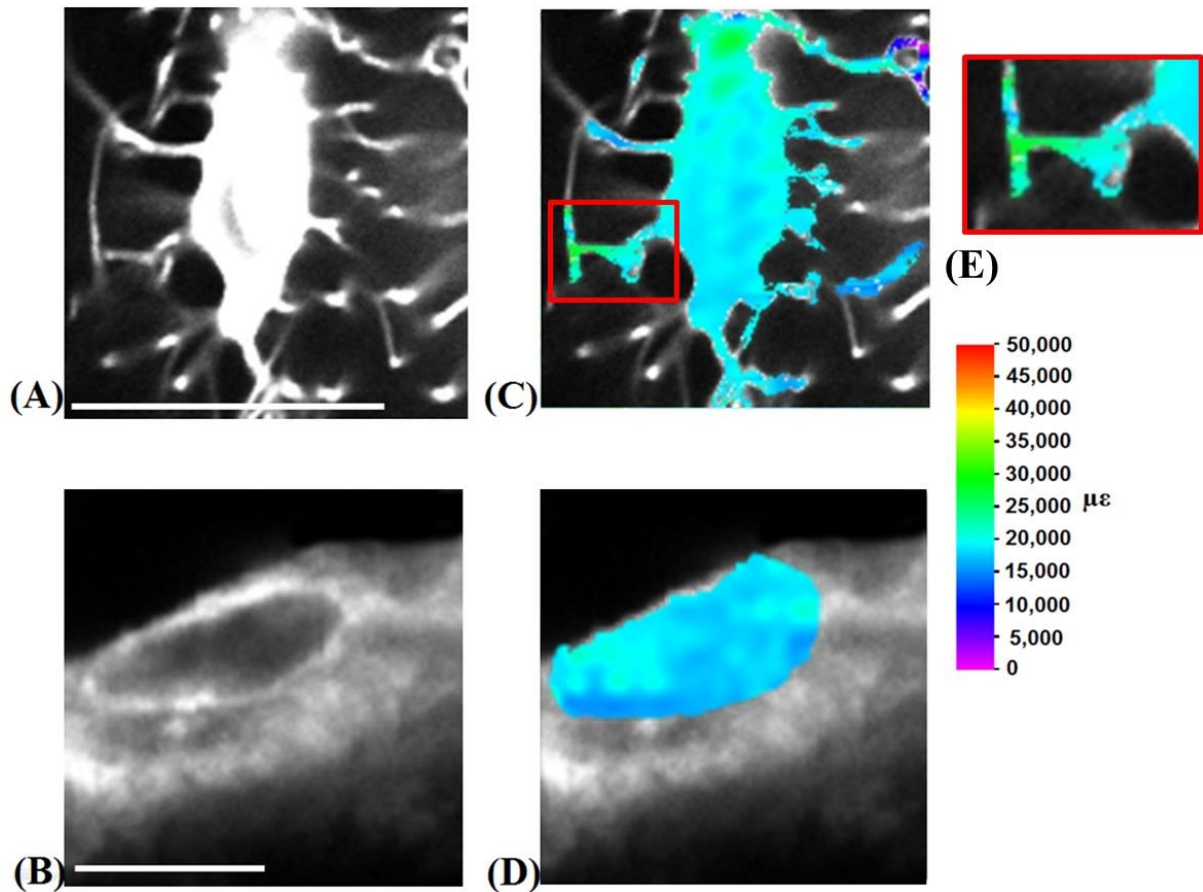
15 **3. RESULTS**

16 **3.1. Mechanical environment of osteoblasts and osteocytes in healthy bone**

17 The strain distribution experienced by a sample osteoblast and sample osteocyte as a result of
18 the applied loading is shown in Fig. 5 (C, D). The strains experienced by these cells, as a
19 proportion of the cell area, are shown in Fig. 6 and Fig. 7 respectively. Strains experienced by
20 osteoblasts from healthy bone exceeded the osteogenic strain threshold (10,000 $\mu\epsilon$) in a larger
21 proportion of the cell ($13.68 \pm 1.31\%$) than osteocytes ($5.37 \pm 2.08\%$), while no significant
22 difference was seen for proportions strained below 1,000 $\mu\epsilon$. Maximum strains experienced
23 by osteoblasts in healthy bone were 24,921 $\mu\epsilon$ ($24,921 \pm 3,832 \mu\epsilon$), with healthy osteocytes
24 experiencing strains of 31,028 $\mu\epsilon$ ($31,028 \pm 4,213 \mu\epsilon$).

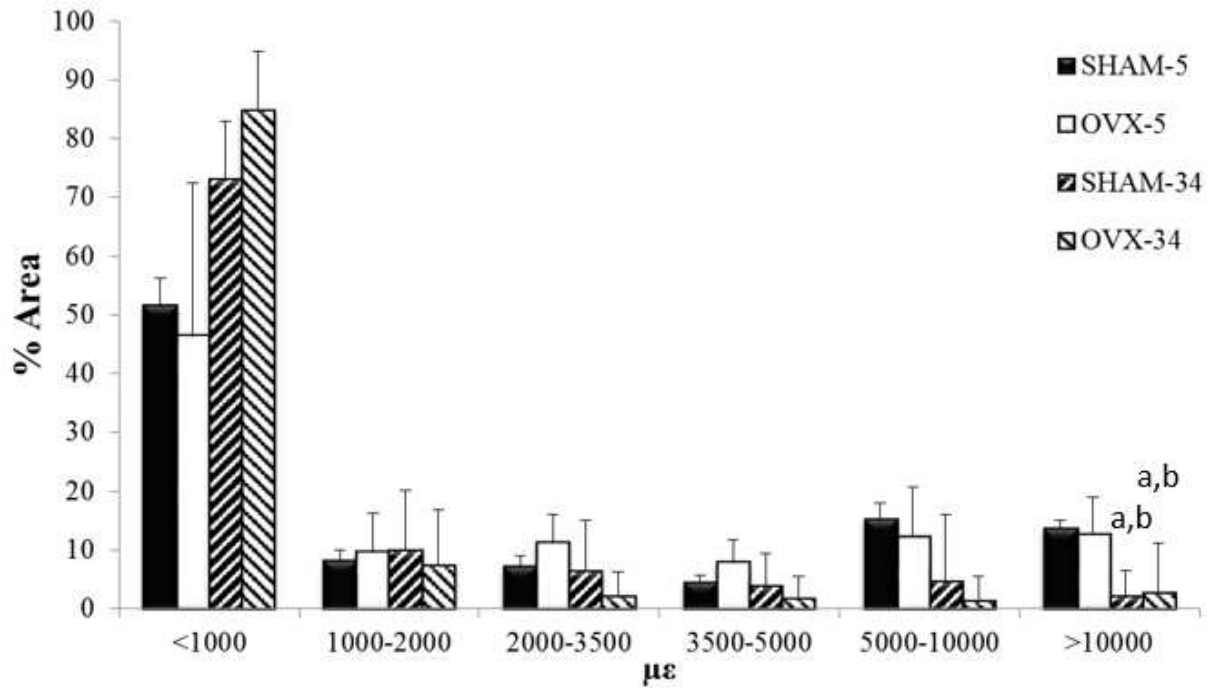
25

26



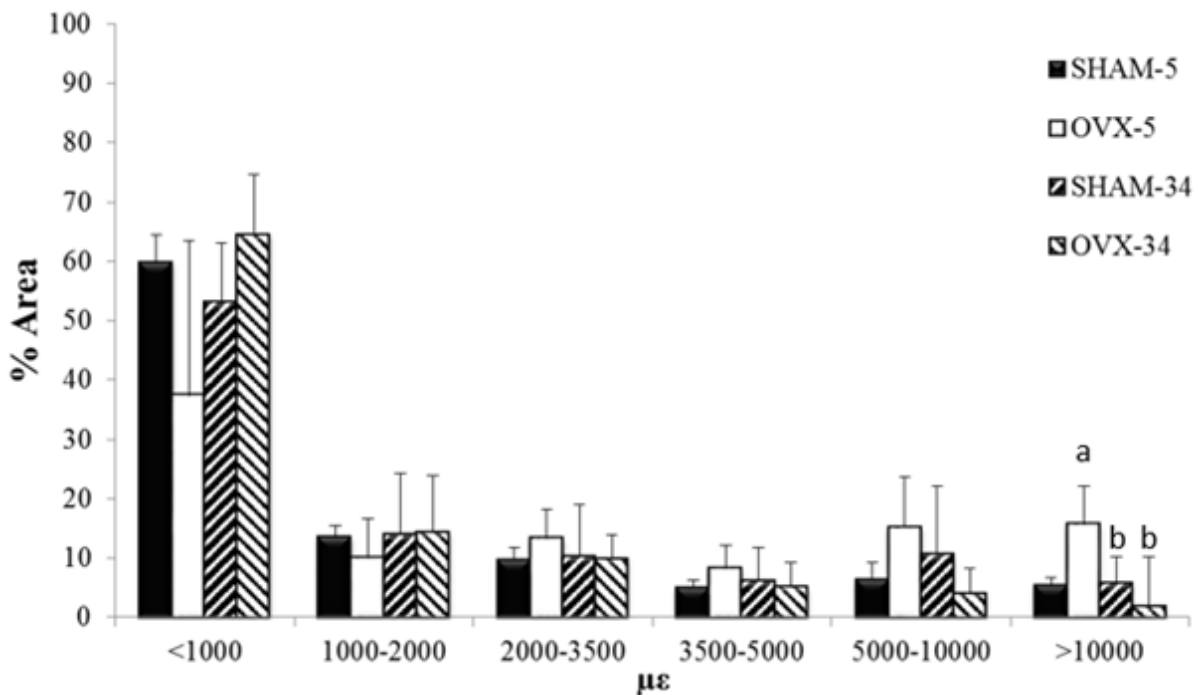
1
2 **FIGURE 5: Confocal images of (A) a sample osteocyte and (B) osteoblast at 0 $\mu\epsilon$. Digital**
3 **image correlation (DIC) is applied to characterise the maximum principal strain**
4 **distribution in (C) the osteocyte, (D) the osteoblast at 3,000 $\mu\epsilon$ (scale bar: 10 μm) and**
5 **(E) strain amplification in an osteocyte cell process.**

6
7 A drop in the proportion of the cell exceeding the osteogenic strain threshold (10,000 $\mu\epsilon$)
8 occurs in osteoblasts ($2.16 \pm 4.39\%$ vs. $13.68 \pm 1.31\%$, $p \leq 0.025$) at 34 weeks after the
9 SHAM operation. However, there was no significant change in this value for osteocytes, at
10 ($5.77 \pm 2.60\%$ vs. $5.37 \pm 2.08\%$). Similarly, there was no significant difference in strains
11 $<1,000 \mu\epsilon$ between these time points, for either osteoblasts or osteocytes.



1

2 **FIGURE 6: Average maximum principal strain distributions observed after 5 and 34**
 3 **weeks in osteoporotic (OVX) and healthy (SHAM) osteoblasts as a percentage of cell**
 4 **area. n=4 for 5 week groups, n=2 for 34 week group, ^a $p < 0.05$ versus SHAM-5 at**
 5 **corresponding strain level, ^b $p < 0.05$ versus OVX-5 at corresponding strain level**



6

7 **FIGURE 7: Average maximum principal strain distributions observed after 5 and 34**
 8 **weeks in osteoporotic (OVX) and healthy (SHAM) osteocytes as a percentage of cell**

1 **area. n=4 for 5 week groups, n=2 for 34 week group, ^a $p < 0.05$ versus SHAM-5 at**
2 **corresponding strain level, ^b $p < 0.05$ versus OVX-5 at corresponding strain level**

3 Contour plots showed greater variability in strain at the cell membranes than within the cell
4 body for all cell types. This effect was exacerbated in the osteocyte environment, with a more
5 heterogeneous distribution and the highest and lowest strains occurring within the cell
6 processes.

7 **3.2. Mechanical environment of osteoblasts and osteocytes during osteoporosis**

8 The effect of osteoporosis on strain within bone cells was examined, with the strain
9 distribution for OVX and SHAM samples compared in Fig. 6 for osteoblasts and Fig. 7 for
10 osteocytes. While it could be seen that strains below 1,000 $\mu\epsilon$ occur in a smaller proportion of
11 osteoporotic osteocytes compared to healthy osteocytes ($37.33 \pm 14.81\%$ vs. $59.77 \pm$
12 10.12%), this difference was not statistically significant ($p \leq 0.095$). Strains exceeding the
13 osteogenic strain threshold (10,000 $\mu\epsilon$) in osteoblasts in bones exposed to 5 weeks of
14 oestrogen deficiency occur in a similar proportion of the cell to healthy bone at 5 weeks
15 ($12.68 \pm 6.30\%$ vs. $13.68 \pm 1.31\%$). However, strains exceeding the osteogenic strain
16 threshold occur in a significantly larger proportion of osteocytes at 5 weeks of oestrogen
17 deficiency compared to healthy osteocytes ($15.74 \pm 2.86\%$ vs. $5.37 \pm 2.08\%$, $p \leq 0.048$). In
18 addition, osteoporotic osteoblasts exhibited maximum strains of 24,585 $\mu\epsilon$ ($24,585 \pm 3,399$
19 $\mu\epsilon$) while osteocytes experienced 40,548 $\mu\epsilon$ ($40,548 \pm 6,041 \mu\epsilon$).

20 After 34 weeks of oestrogen deficiency, the proportion of osteoblast and osteocyte cell areas
21 experiencing strains above the osteogenic threshold is significantly lower than osteoblasts
22 ($2.71 \pm 8.36\%$ vs. $12.68 \pm 6.30\%$, $p \leq 0.025$) and osteocytes ($1.83 \pm 2.24\%$ vs. $15.74 \pm$
23 2.86% , $p \leq 0.039$) at 5 weeks oestrogen deficiency. Furthermore, there was no significant
24 difference between osteoporotic cells and healthy cells after 34 weeks post-operation for
25 either osteoblasts ($2.71 \pm 8.36\%$ vs. $2.16 \pm 4.39\%$) or osteocytes ($2.71 \pm 8.36\%$ vs. $5.77 \pm$
26 2.60%). Similarly, there was no significant difference between maximum strains in
27 osteoporotic and healthy cells at 34 weeks post-operation for either osteoblasts ($14,731 \pm$
28 $1,840 \mu\epsilon$ vs. $16,541 \pm 1,930 \mu\epsilon$) or osteocytes ($14,474 \pm 1,446 \mu\epsilon$ vs. $19,195 \pm 3,204 \mu\epsilon$).

29 Similar to the contour plots of the healthy cells, the highest and lowest strains occurred at the
30 cell membranes of both cell types, particularly in the cell processes of osteocytes. The strain
31 behaviour within osteoblasts and osteocytes was not found to vary between osteoporotic or
32 normal bone cells.

33 Finally, due to the stepped nature of the loading it is possible to capture results for lower
34 levels of applied strain. In order to determine if cellular deformation in response to applied
35 loading was non-linear, strains in osteocytes from the SHAM and OVX groups at 5 weeks
36 were investigated, from 0 to 1,500 $\mu\epsilon$. At 1,500 $\mu\epsilon$, maximum strains within the osteocytes
37 were approximately half of those observed at 3,000 $\mu\epsilon$ (SHAM: 14,400 $\mu\epsilon$ vs 31,028 $\mu\epsilon$;
38 OVX: 22,040 $\mu\epsilon$ vs. 40,548 $\mu\epsilon$). This indicates that while loading of osteocytes is amplified
39 at the cell level, it increases proportional to the applied macroscopic load.

1

2 4. DISCUSSION

3 This study represents the first direct experimental investigation of the changes in the local
4 mechanical environment of osteocytes and osteoblasts in situ during oestrogen deficiency. By
5 characterising the strain distribution within cells using a rat model of osteoporosis, we report
6 for the first time that osteoblasts and osteocytes in both healthy and osteoporotic bone
7 experience strains that are sufficient to stimulate osteogenic responses ($>10,000 \mu\epsilon$) under
8 physiological loading conditions. However, while osteocytes in osteoporotic bone initially (5
9 weeks post-operation) experience osteogenic strains ($>10,000 \mu\epsilon$) in a greater area of the cell
10 (10%) than those in healthy bone, there is no significant difference for osteoblasts. In
11 contrast, in long-term oestrogen deficiency (34 weeks post-operation) there is a significant
12 decrease in the proportion of both osteoblasts and osteocytes exceeding the osteogenic strain
13 threshold ($>10,000 \mu\epsilon$) compared to the respective cells at 5 weeks oestrogen deficiency,
14 such that there is no longer a significant difference between either osteoblasts or osteocytes in
15 34-week osteoporotic and healthy bone.

16 One limitation of this study is that the confocal microscopy imaging and DIC approach
17 limited the analysis to 2D sections of individual cells, and as such it was assumed that the
18 strains experienced within that cell section are representative of the strains experienced by the
19 whole cell. Immunohistochemistry was not performed to identify the phenotype of the cells.
20 However, their locations were chosen to represent the local mechanical environment of
21 osteoblasts (but also quiescent osteoblasts (bone lining cells)) and osteocytes. It should be
22 noted that not all animals survived to 34 weeks post-OVX, reducing the number of animals
23 per group at this time point ($n=2$ per group). Nonetheless, significant differences were
24 observed in stimulation of cells between animal groups at the 5 week time point, but future
25 studies should investigate the temporal nature of changes in the mechanical environment of
26 bone cells with an animal model that displayed the time-sequence of the complex changes in
27 all of these tissue parameters. Interstitial fluid flow and movement out of plane due to loading
28 cannot be quantified directly using DIC, and, due to the time required to capture the scans
29 between each load step, any time-dependent or flow-induced deformation could not be
30 specifically delineated. Similarly, it was also not possible to measure the micro-scale strains
31 in the surrounding bone directly using DIC, as the bone matrix was not fluorescent under
32 confocal laser scanning microscopy. As such the role of specific stimuli, such as fluid flow or
33 matrix strain, cannot be distinguished but likely all contribute to the strains reported here due
34 to the efforts to maintain the in vivo mechanical environment in our experiment. The strain
35 amplification observed at the cell surfaces is unlikely to be an artefact of the DIC approach,
36 as no similar amplification is visible at the surface of the microspheres, despite the clear
37 boundary between it and the surrounding matrix. Moreover, such concentrations of strain
38 along the cell surfaces and cell processes of osteocytes, with lower strains in the cell body,
39 have been predicted by multiple modelling approaches (27, 47, 48). Therefore we conclude
40 that the imaging and analysis approaches are robust enough to accurately predict strain in

1 bone cells. Indeed, our method represents the first approach to elucidate cellular strains in
2 their local mechanical environment without destructive interference.

3 It should also be noted that the cutting procedure exposed the bone marrow cavity and the
4 resulting drop in intramedullary pressure may alter interstitial fluid flow within the bone (49,
5 50). However, the samples were kept moist during loading using PBS and the periosteum was
6 maintained intact on the outer surface of the bone. Furthermore, the flow velocities are
7 extremely low within the lacunar-canalicular network ($\sim 60 \mu\text{m/s}$) (48, 51), and are therefore
8 unlikely to be altered significantly away from the cut surfaces. It is important to note that the
9 type of mechanical stimulation bone cells experience in vivo has been unclear to date, and as
10 such whether the cells respond to peak strains or overall stimulation of a proportion of the
11 cell body is unknown. For this reason we reported both peak strains and the percentage of cell
12 area experiencing specific strain magnitudes, and compared these to an assumed osteogenic
13 threshold of $10,000 \mu\epsilon$. This threshold was chosen based on the findings of various
14 experimental, computational and theoretical studies of osteocytes and osteoblasts (19-23), in
15 particular an in vitro cell culture study that reported significant osteogenic responses in
16 osteoblastic cells at magnitudes greater than a threshold of approximately $10,000 \mu\epsilon$ (6, 24).
17 Future development of confocal laser scanning techniques may be able to better observe the
18 mechanical behaviour of the cell during loading, and could be combined with fluorescent
19 studies of calcium and nitric oxide signally in bone cell networks to determine stimulatory
20 strain levels in vivo (52-55).

21 Previous experimental studies of bone cell mechanobiology have largely involved in
22 vitro cell culture techniques (4-6, 22, 23). We report maximum strains in healthy osteocytes
23 in situ of approximately $31,000 \mu\epsilon$, far in excess of the applied loading of $3,000 \mu\epsilon$. These
24 results corroborate experimentally observed strain amplification ($35,000 \mu\epsilon$) in the lacunar
25 matrix (20, 21) and verify the importance of predicted strain amplification in osteocytes by a
26 glycocalyx or integrin attachments to the matrix (27, 56-58). Our results show that
27 osteoblasts in healthy bone are stimulated to a greater extent than osteocytes (based on
28 proportion of the cell above $10,000 \mu\epsilon$). Osteoblasts are exposed to surface bending (59) and
29 marrow shear stress (60, 61), and are also connected to the bone surface and other cells by
30 discrete attachments (62, 63). Indeed, recent computational studies of the bone marrow cavity
31 have predicted that high shear stresses act along bone surfaces, at magnitudes that have been
32 observed to stimulate bone cells in vitro (60). These factors may account for the amplified
33 osteoblast stimulation observed in the current study. Despite the greater strain stimulation of
34 osteoblasts observed here, the osteocyte likely experiences both direct strain from the bone
35 matrix as well as an additional stimulus resulting from loading-induced interstitial fluid flow
36 (48), to which osteocytes are highly responsive (3, 64). Interestingly, in the current study
37 osteocytes experienced greater maximum strains than osteoblasts, and it is noteworthy that
38 these stimuli occurred along the cell processes, known to be the most mechanosensitive area
39 of the osteocyte (32, 65).

40 Of particular interest in this study are the precise changes that occur during early-
41 stage oestrogen deficiency that may alter the mechanical environment of bone cells. At the

1 onset of osteoporosis micro-structural changes in bone strength (9, 10), mass (8), mineral
2 density (9, 16, 66), trabecular architecture (8, 10, 66), and trabecular mineral and matrix
3 composition (9, 10, 14, 66) occur. Previous studies have observed changes in the geometry of
4 the osteocyte lacunar-canalicular environment occur during oestrogen-deficiency (11-13).
5 ImageJ image analysis software was used to calculate circularity of each cell body (i.e. the
6 degree of roundness) analysed in this study, but the results indicated that there was no
7 statistical difference between the circularity of SHAM (0.2779 ± 0.1236) and OVX
8 osteocytes (0.2277 ± 0.1418), $p = 0.434$. While we have not observed a difference in the
9 dimensions of the cell body during oestrogen deficiency, previous studies have observed and
10 quantified changes in the lacunar-canalicular anatomy (11-13, 67), and these may play a role
11 in the stimulation changes observed here. Additionally, a recent computational study by our
12 group demonstrated that mechanical stimulation of osteocytes can differ vastly depending on
13 location within the extracellular matrix, particularly in relation to micropores (47). This may
14 be important during oestrogen-deficiency, as porosity has been observed to increase
15 significantly in an ovine model of osteoporosis (68). Furthermore, oestrogen treatment has
16 recently been observed to cause significant decreases in osteoblast cytoskeletal stiffness (69),
17 and such changes might play a role in the altered mechanical stimulation reported here. Our
18 experimental method maintains all aspects of the local mechanical environment of bone cells,
19 including the composition of the extracellular and pericellular matrix, the geometry of the
20 lacunar-canalicular network, physical connections between the cell and its surroundings, the
21 cell mechanical behaviour, and the in vivo mechanical stimuli arising from loading-induced
22 fluid flow and matrix strain. Therefore, any of these complex changes in structure and
23 composition could dictate the changes in cellular strains reported here.

24 It is intriguing to speculate on the temporal changes in mechanical stimulation of bone
25 cells during osteoporosis observed here. While theories have been proposed as to the
26 mechanisms that cause osteoporosis (70, 71), here we delineate the timeline of observed
27 events in order to gain an insight into the development of the disease. In a rat model of
28 osteoporosis, osteoclastogenesis increases significantly as early as 1 week post-OVX (72),
29 resulting in decreased bone volume fraction and trabecular number by 4 weeks post-OVX
30 (73). This initial bone loss likely alters the micromechanical loading of bone cells, but this
31 has never before been demonstrated. Our results show for the first time that osteocytes
32 experience higher strains in osteoporotic bone than in healthy bone by 5 weeks post-OVX,
33 thus verifying that early bone loss increases the stimulation of osteocytes in the remaining
34 bone. Significant increases in trabecular thickness (74, 75) and stiffness (14) occur at later
35 time points in rats, at 14 and 34 weeks post-OVX, which might explain our observations of
36 restoration of the strain environment of osteocytes to control levels in late-stage osteoporosis
37 (34 weeks post-OVX). It was also observed that osteoblasts and osteocytes experienced
38 strains below $1,000 \mu\epsilon$, levels believed to initiate disuse-related bone resorption (76). This
39 likely occurs due to a strain-shielding effect whereby the pericellular matrix (PCM) reduces
40 strain transfer to the cell, a phenomenon that has been predicted in computational models of
41 osteocytes and chondrocytes (27, 77, 78). Interestingly, it was seen that the percentage area of
42 osteoporotic cells experiencing such strains at 5 weeks post-OVX was lower than controls at

1 the same time point, whereas at 34 weeks post-OVX such strains were more prevalent in
2 osteoporotic bone cells than control cells. While these observations were not statistically
3 significant, when coupled with those of the osteogenic stimulation they suggest that during
4 the initial stage of osteoporosis, bone cells experience a decreased resorption stimulus and an
5 increased osteogenic stimulus, but that this effect is diminished during late-stage
6 osteoporosis. Furthermore, studies of ovine trabecular and cortical bone reported an initial
7 significant decrease (12 months post-OVX) in mineral content and elastic modulus relative to
8 controls, but that these properties and compressive strength matched control levels in long-
9 term oestrogen deficiency (31 months post-OVX) despite continued increases in porosity and
10 turnover (9, 79). Therefore, although the timing of changes in tissue properties appears to
11 vary between animal models, there is a clear trend of early bone loss followed by increases in
12 tissue stiffness to return properties to control levels. Taken together with results of the current
13 study, these experimental observations of temporal changes in both cortical and trabecular
14 bone support the theory that a compensatory mechanobiological response occurs during later
15 stage osteoporosis to counter altered tissue mechanics due to oestrogen deficiency (80).

16 Finally, it is important to note that the results of the study may differ to the human
17 disease of osteoporosis, as specific differences exist between the rat and human bone biology,
18 including the rare occurrence of Basic Multicellular Unit (BMU) remodelling in rat bone
19 (81), as well as the apparent absence of classic Haversian systems, or osteons (44).
20 Nonetheless the ovariectomised rat is an established model of post-menopausal osteoporosis
21 in humans that is commonly used due to the fact that the model displays many of the same
22 characteristics, such as increased rate of bone turnover with absorption exceeding formation
23 (82, 83), greater decrease in trabecular bone compared to cortical bone (82-84), decreased
24 calcium absorption (82, 85, 86), and similar skeletal responses to drug treatments and
25 exercise (87-90). Therefore the overall remodelling activity of rat bone bears remarkable
26 similarities to that of human bone (91) and, as such, the results of this study provide novel
27 information that might inform future study of the human bone disease of osteoporosis.

28 **5. CONCLUSIONS**

29 In summary, we report experimental evidence that osteocytes in healthy bone tissue
30 experience higher maximum strains ($31,028 \pm 4,213 \mu\epsilon$) than osteoblasts ($24,921 \pm 3,832 \mu\epsilon$),
31 whereas osteoblasts experience elevated strains ($> 10,000 \mu\epsilon$) throughout a greater proportion
32 of their cell body than osteocytes. Most interestingly we show that, in early-stage
33 osteoporosis, osteocytes sense osteogenic strain magnitudes in a greater proportion of the cell
34 (10%), with 23% greater maximum strains, than healthy cells. However we also observe that,
35 in late-stage osteoporosis, cellular strains in both cell types decrease significantly compared
36 to early-stage osteoporosis, such that there is no significant difference between bone cells in
37 healthy and normal bone. This suggests that a mechanobiological response may have
38 occurred to alter the mechanical environment, perhaps in an attempt to restore homeostasis.
39 This study provides a greater understanding of the mechanobiology of bone cells during the
40 disease of osteoporosis.

1 6. ACKNOWLEDGEMENTS

2 The authors would like to acknowledge funding from the Irish Research Council (IRC), under
3 the EMBARK program (S. W. V.) and the European Research Council (ERC) under grant
4 number 258992 (BONEMECHBIO).

5

6 7. REFERENCES

- 7 1. Birmingham E, GL Niebur, PE McHugh, G Shaw, FP Barry, LM McNamara.
8 Osteogenic differentiation of mesenchymal stem cells is regulated by osteocyte and
9 osteoblast cells in a simplified bone niche. *Eur Cell Mater.* 2012;23:13-27.
- 10 2. Jahani M, PG Genever, RJ Patton, F Ahwal, MJ Fagan. The effect of osteocyte
11 apoptosis on signalling in the osteocyte and bone lining cell network: a computer simulation.
12 *Journal of Biomechanics.* 2012;45(16):2876-83.
- 13 3. Klein-Nulend J, A van der Plas, CM Semeins, NE Ajubi, JA Frangos, PJ Nijweide, et
14 al. Sensitivity of osteocytes to biomechanical stress in vitro. *The FASEB Journal.* 1995
15 March 1, 1995;9(5):441-5.
- 16 4. Owan I, DB Burr, CH Turner, J Qiu, Y Tu, JE Onyia, et al. Mechanotransduction in
17 bone: osteoblasts are more responsive to fluid forces than mechanical strain. *American*
18 *Journal of Physiology - Cell Physiology.* 1997 September 1, 1997;273(3):C810-C5.
- 19 5. Smalt R, FT Mitchell, RL Howard, TJ Chambers. Induction of NO and prostaglandin
20 E2 in osteoblasts by wall-shear stress but not mechanical strain. *American Journal of*
21 *Physiology - Endocrinology And Metabolism.* 1997 October 1, 1997;273(4):E751-E8.
- 22 6. You J, CE Yellowley, HJ Donahue, Y Zhang, Q Chen, CR Jacobs. Substrate
23 Deformation Levels Associated With Routine Physical Activity Are Less Stimulatory to
24 Bone Cells Relative to Loading-Induced Oscillatory Fluid Flow. *Journal of Biomechanical*
25 *Engineering.* 2000;122(4):387-93.
- 26 7. Braidman IP, L Hainey, G Batra, PL Selby, PTK Saunders, JA Hoyland. Localization
27 of Estrogen Receptor β Protein Expression in Adult Human Bone. *Journal of Bone and*
28 *Mineral Research.* 2001;16(2):214-20.
- 29 8. Lane NE, JM Thompson, D Haupt, DB Kimmel, G Modin, JH Kinney. Acute
30 Changes in Trabecular Bone Connectivity and Osteoclast Activity in the Ovariectomized Rat
31 *In Vivo.* *Journal of Bone and Mineral Research.* 1998;13(2):229-36.
- 32 9. Brennan O, OD Kennedy, TC Lee, SM Rackard, FJ O'Brien, LM McNamara. The
33 effects of estrogen deficiency and bisphosphonate treatment on tissue mineralisation and
34 stiffness in an ovine model of osteoporosis. *Journal of Biomechanics.* 2011;44(3):386-90.
- 35 10. Brennan O, J Kuliwaba, TC Lee, I Parkinson, N Fazzalari, L McNamara, et al.
36 Temporal Changes in Bone Composition, Architecture, and Strength Following Estrogen
37 Deficiency in Osteoporosis. *Calcif Tissue Int.* 2012 2012/12/01;91(6):440-9.
- 38 11. Knothe Tate ML, JR Adamson, AE Tami, TW Bauer. The osteocyte. *The*
39 *International Journal of Biochemistry & Cell Biology.* 2004;36(1):1-8.

- 1 12. KnotheTate M, A Tami, T Bauer, U Knothe. Micropathoanatomy of osteoporosis:
2 indications for a cellular basis of bone disease. *Advances in Osteoporotic Fracture*
3 *Management*. 2002;2(1):9-14.
- 4 13. Sharma D, C Ciani, PAR Marin, JD Levy, SB Doty, SP Fritton. Alterations in the
5 osteocyte lacunar–canalicular microenvironment due to estrogen deficiency. *Bone*.
6 2012;51(3):488-97.
- 7 14. McNamara LM, AGH Ederveen, CG Lyons, C Price, MB Schaffler, H Weinans, et al.
8 Strength of cancellous bone trabecular tissue from normal, ovariectomized and drug-treated
9 rats over the course of ageing. *Bone*. 2006;39(2):392-400.
- 10 15. McNamara LM, PJ Prendergast. Perforation of cancellous bone trabeculae by
11 damage-stimulated remodelling at resorption pits: a computational analysis. *Eur J Morphol*.
12 2005 Feb-Apr;42(1-2):99-109.
- 13 16. Brennan MA, JP Gleeson, M Browne, FJ O'Brien, PJ Thurner, LM McNamara. Site
14 specific increase in heterogeneity of trabecular bone tissue mineral during oestrogen
15 deficiency. *Eur Cell Mater*. 2011;21:396-406.
- 16 17. Van Der Linden JC, J Homminga, JAN Verhaar, H Weinans. Mechanical
17 Consequences of Bone Loss in Cancellous Bone. *Journal of Bone and Mineral Research*.
18 2001;16(3):457-65.
- 19 18. Mulvihill BM, LM McNamara, PJ Prendergast. Loss of trabeculae by mechano-
20 biological means may explain rapid bone loss in osteoporosis. *Journal of The Royal Society*
21 *Interface*. 2008 October 6, 2008;5(27):1243-53.
- 22 19. Nicolella DP, AE Nicholls, J Lankford, DT Davy. Machine vision photogrammetry: a
23 technique for measurement of microstructural strain in cortical bone. *Journal of*
24 *Biomechanics*. [doi: 10.1016/S0021-9290(00)00163-9]. 2001;34(1):135-9.
- 25 20. Nicolella DP, LF Bonewald, DE Moravits, J Lankford. Measurement of
26 microstructural strain in cortical bone. *European Journal of Morphology*. [Article].
27 2005;42(1/2):23-9.
- 28 21. Nicolella DP, DE Moravits, AM Gale, LF Bonewald, J Lankford. Osteocyte lacunae
29 tissue strain in cortical bone. *Journal of Biomechanics*. [doi:
30 10.1016/j.jbiomech.2005.04.032]. 2006;39(9):1735-43.
- 31 22. Charras GT, MA Horton. Determination of Cellular Strains by Combined Atomic
32 Force Microscopy and Finite Element Modeling. *Biophysical Journal*. 2002;83(2):858-79.
- 33 23. Charras GT, PP Lehenkari, MA Horton. Atomic force microscopy can be used to
34 mechanically stimulate osteoblasts and evaluate cellular strain distributions. *Ultramicroscopy*.
35 2001;86(1–2):85-95.
- 36 24. Burger EH, JP Veldhuijzen. Influence of mechanical factors on bone formation,
37 resorption and growth in vitro. Hall BK, editor: CRC Press Boca Raton, FL.; 1993.
- 38 25. Reilly GC. Observations of microdamage around osteocyte lacunae in bone. *Journal*
39 *of Biomechanics*. 2000;33(9):1131-4.
- 40 26. Zioupos P, JD Currey. The extent of microcracking and the morphology of
41 microcracks in damaged bone. *Journal of Materials Science*. 1994;29(4):978-86.

- 1 27. Verbruggen SW, TJ Vaughan, LM McNamara. Strain amplification in bone
2 mechanobiology: a computational investigation of the in vivo mechanics of osteocytes.
3 *Journal of The Royal Society Interface*. 2012 June 6, 2012.
- 4 28. Ciani C, SB Doty, SP Fritton. An effective histological staining process to visualize
5 bone interstitial fluid space using confocal microscopy. *Bone*. [doi:
6 10.1016/j.bone.2009.01.376]. 2009;44(5):1015-7.
- 7 29. Price C, W Li, JE Novotny, L Wang. An in-situ fluorescence-based optical
8 extensometry system for imaging mechanically loaded bone. *Journal of Orthopaedic*
9 *Research*. 2010;28(6):805-11.
- 10 30. Wang L, SC Cowin, S Weinbaum, SP Fritton. Modeling Tracer Transport in an
11 Osteon under Cyclic Loading. *Annals of Biomedical Engineering*. 2000;28(10):1200-9.
- 12 31. Zhou X, J Novotny, L Wang. Modeling Fluorescence Recovery After Photobleaching
13 in Loaded Bone: Potential Applications in Measuring Fluid and Solute Transport in the
14 Osteocytic Lacunar-Canalicular System. *Annals of Biomedical Engineering*. 2008
15 2008/12/01;36(12):1961-77.
- 16 32. Adachi T, Y Aonuma, M Tanaka, M Hojo, T Takano-Yamamoto, H Kamioka.
17 Calcium response in single osteocytes to locally applied mechanical stimulus: Differences in
18 cell process and cell body. *Journal of Biomechanics*. [doi: 10.1016/j.jbiomech.2009.04.034].
19 2009;42(12):1989-95.
- 20 33. Kamioka H, T Honjo, T Takano-Yamamoto. A three-dimensional distribution of
21 osteocyte processes revealed by the combination of confocal laser scanning microscopy and
22 differential interference contrast microscopy. *Bone*. 2001;28(2):145-9.
- 23 34. Kamioka H, Y Sugawara, SA Murshid, Y Ishihara, T Honjo, T Takano-Yamamoto.
24 Fluid Shear Stress Induces Less Calcium Response in a Single Primary Osteocyte Than in a
25 Single Osteoblast: Implication of Different Focal Adhesion Formation. *Journal of Bone and*
26 *Mineral Research*. 2006;21(7):1012-21.
- 27 35. Sugawara Y, H Kamioka, T Honjo, K-i Tezuka, T Takano-Yamamoto. Three-
28 dimensional reconstruction of chick calvarial osteocytes and their cell processes using
29 confocal microscopy. *Bone*. 2005;36(5):877-83.
- 30 36. Sugawara Y, H Kamioka, Y Ishihara, N Fujisawa, N Kawanabe, T Yamashiro. The
31 early mouse 3D osteocyte network in the presence and absence of mechanical loading. *Bone*.
32 2013;52(1):189-96.
- 33 37. Bruehlmann SB, JR Matyas, NA Duncan. ISSLS Prize Winner: Collagen Fibril
34 Sliding Governs Cell Mechanics in the Anulus Fibrosus: An In Situ Confocal Microscopy
35 Study of Bovine Discs. *Spine*. 2004;29(23):2612-20 10.1097/01.brs.0000146465.05972.56.
- 36 38. Villemure I, L Cloutier, JR Matyas, NA Duncan. Non-uniform strain distribution
37 within rat cartilaginous growth plate under uniaxial compression. *Journal of Biomechanics*.
38 2007;40(1):149-56.
- 39 39. Luu L, Z Wang, M Vo, T Hoang, J Ma. Accuracy enhancement of digital image
40 correlation with B-spline interpolation. *Opt Lett*. 2011;36(16):3070-2.
- 41 40. Pan B, Z Wang, Z Lu. Genuine full-field deformation measurement of an object with
42 complex shape using reliability-guided digital image correlation. *Opt Express*.
43 2010;18(2):1011-23.

- 1 41. Pan B, H Xie, Z Wang. Equivalence of digital image correlation criteria for pattern
2 matching. *Appl Opt.* 2010;49(28):5501-9.
- 3 42. Bilgen M, MF Insana. Elastostatics of a spherical inclusion in homogeneous
4 biological media. *Physics in Medicine and Biology.* 1998;43(1):1.
- 5 43. World-Health-Organization. Guidelines for preclinical evaluation and clinical trials in
6 osteoporosis. Geneva, Switzerland: World Health Organization; 1998.
- 7 44. Kalu DN. The ovariectomized rat model of postmenopausal bone loss. *Bone and*
8 *Mineral.* 1991;15(3):175-91.
- 9 45. McNamara L, J Van der Linden, H Weinans, P Prendergast. Stress-concentrating
10 effect of resorption lacunae in trabecular bone. *Journal of Biomechanics.* 2006;39(4):734-41.
- 11 46. McNamara LM, PJ Prendergast. Bone remodelling algorithms incorporating both
12 strain and microdamage stimuli. *Journal of Biomechanics.* 2007;40(6):1381-91.
- 13 47. Vaughan TJ, SW Verbruggen, LM McNamara. Are all osteocytes equal? Multiscale
14 modelling of cortical bone to characterise the mechanical stimulation of osteocytes.
15 *International Journal for Numerical Methods in Biomedical Engineering.* 2013:n/a-n/a.
- 16 48. Verbruggen S, T Vaughan, L McNamara. Fluid flow in the osteocyte mechanical
17 environment: a fluid–structure interaction approach. *Biomech Model Mechanobiol.* 2013
18 2013/04/09:1-13.
- 19 49. Hu M, J Cheng, N Bethel, F Serra-Hsu, S Ferreri, L Lin, et al. Interrelation between
20 external oscillatory muscle coupling amplitude and *i* in vivo *i* intramedullary pressure
21 related bone adaptation. *Bone.* 2014;66:178-81.
- 22 50. Qin Y-X, T Kaplan, A Saldanha, C Rubin. Fluid pressure gradients, arising from
23 oscillations in intramedullary pressure, is correlated with the formation of bone and inhibition
24 of intracortical porosity. *Journal of Biomechanics.* 2003;36(10):1427-37.
- 25 51. Price C, X Zhou, W Li, L Wang. Real-time measurement of solute transport within
26 the lacunar-canalicular system of mechanically loaded bone: Direct evidence for load-
27 induced fluid flow. *Journal of Bone and Mineral Research.* 2011;26(2):277-85.
- 28 52. Jing D, XL Lu, E Luo, P Sajda, PL Leong, XE Guo. Spatiotemporal properties of
29 intracellular calcium signaling in osteocytic and osteoblastic cell networks under fluid flow.
30 *Bone.* 2013;53(2):531-40.
- 31 53. Lu XL, B Huo, V Chiang, XE Guo. Osteocytic network is more responsive in calcium
32 signaling than osteoblastic network under fluid flow. *Journal of Bone and Mineral Research.*
33 2012;27(3):563-74.
- 34 54. Lu XL, B Huo, M Park, XE Guo. Calcium response in osteocytic networks under
35 steady and oscillatory fluid flow. *Bone.* 2012;51(3):466-73.
- 36 55. Vatsa A, TH Smit, J Klein-Nulend. Extracellular NO signalling from a mechanically
37 stimulated osteocyte. *Journal of Biomechanics.* 2007;40, Supplement 1(0):S89-S95.
- 38 56. Han Y, SC Cowin, MB Schaffler, S Weinbaum. Mechanotransduction and strain
39 amplification in osteocyte cell processes. *Proceedings of the National Academy of Sciences*
40 *of the United States of America.* 2004 November 23, 2004;101(47):16689-94.
- 41 57. Vaughan TJ, CA Mullen, SW Verbruggen, LM McNamara. Bone cell
42 mechanosensation of fluid flow stimulation: a fluid–structure interaction model

1 characterising the role integrin attachments and primary cilia. *Biomech Model Mechanobiol.*
2 2014 2014/11/16:1-16.

3 58. Wang Y, LM McNamara, MB Schaffler, S Weinbaum. A model for the role of
4 integrins in flow induced mechanotransduction in osteocytes. *Proceedings of the National*
5 *Academy of Sciences.* 2007 October 2, 2007;104(40):15941-6.

6 59. Fritton SP, K J. McLeod, CT Rubin. Quantifying the strain history of bone: spatial
7 uniformity and self-similarity of low-magnitude strains. *Journal of Biomechanics.* [doi:
8 10.1016/S0021-9290(99)00210-9]. 2000;33(3):317-25.

9 60. Birmingham E, JA Grogan, GL Niebur, LM McNamara, PE McHugh. Computational
10 Modelling of the Mechanics of Trabecular Bone and Marrow Using Fluid Structure
11 Interaction Techniques. *Annals of Biomedical Engineering.* 2013 2013/04/01;41(4):814-26.

12 61. Coughlin TR, GL Niebur. Fluid shear stress in trabecular bone marrow due to low-
13 magnitude high-frequency vibration. *Journal of Biomechanics.* 2012;45(13):2222-9.

14 62. Grigoriou V, IM Shapiro, EA Cavalcanti-Adam, RJ Composto, P Ducheyne, CS
15 Adams. Apoptosis and Survival of Osteoblast-like Cells Are Regulated by Surface
16 Attachment. *Journal of Biological Chemistry.* 2005 January 21, 2005;280(3):1733-9.

17 63. Shapiro F. Bone development and its relation to fracture repair. The role of
18 mesenchymal osteoblasts and surface osteoblasts. *Eur Cell Mater.* 2008;15:53-76.

19 64. Westbroek I, NE Ajubi, MJ Alblas, CM Semeins, J Klein-Nulend, EH Burger, et al.
20 Differential Stimulation of Prostaglandin G/H Synthase-2 in Osteocytes and Other
21 Osteogenic Cells by Pulsating Fluid Flow. *Biochemical and Biophysical Research*
22 *Communications.* 2000;268(2):414-9.

23 65. Burra S, DP Nicoletta, WL Francis, CJ Freitas, NJ Mueschke, K Poole, et al.
24 Dendritic processes of osteocytes are mechanotransducers that induce the opening of
25 hemichannels. *Proceedings of the National Academy of Sciences.* 2010 August 3,
26 2010;107(31):13648-53.

27 66. Busse B, M Hahn, M Soltau, J Zustin, K Püschel, GN Duda, et al. Increased calcium
28 content and inhomogeneity of mineralization render bone toughness in osteoporosis:
29 Mineralization, morphology and biomechanics of human single trabeculae. *Bone.*
30 2009;45(6):1034-43.

31 67. Lane NE, W Yao, M Balooch, RK Nalla, G Balooch, S Habelitz, et al.
32 Glucocorticoid-Treated Mice Have Localized Changes in Trabecular Bone Material
33 Properties and Osteocyte Lacunar Size That Are Not Observed in Placebo-Treated or
34 Estrogen-Deficient Mice. *Journal of Bone and Mineral Research.* 2006;21(3):466-76.

35 68. Kennedy OD, O Brennan, SM Rackard, A Staines, FJ O'Brien, D Taylor, et al. Effects
36 of ovariectomy on bone turnover, porosity, and biomechanical properties in ovine compact
37 bone 12 months postsurgery. *Journal of Orthopaedic Research.* 2009;27(3):303-9.

38 69. Muthukumaran P, CT Lim, T Lee. Estradiol influences the mechanical properties of
39 human fetal osteoblasts through cytoskeletal changes. *Biochemical and Biophysical Research*
40 *Communications.* 2012;423(3):503-8.

41 70. Lanyon L, T Skerry. Perspective: Postmenopausal Osteoporosis as a Failure of Bone's
42 Adaptation to Functional Loading: A Hypothesis*. *Journal of Bone and Mineral Research.*
43 2001;16(11):1937-47.

- 1 71. Rosen CJ, ML Bouxsein. Mechanisms of disease: is osteoporosis the obesity of bone?
2 Nature Clinical Practice Rheumatology. 2006;2(1):35-43.
- 3 72. Hughes DE, A Dai, JC Tiffée, HH Li, GR Mundy, BF Boyce. Estrogen promotes
4 apoptosis of murine osteoclasts mediated by TGF- β . Nature medicine. 1996;2(10):1132-6.
- 5 73. Keiler AM, O Zierau, G Vollmer, D Scharnweber, R Bernhardt. Estimation of an
6 early meaningful time point of bone parameter changes in application to an osteoporotic rat
7 model with in vivo microcomputed tomography measurements. Laboratory Animals.
8 2012;46(3):237-44.
- 9 74. Waarsing JH, JS Day, JC van der Linden, AG Ederveen, C Spanjers, N De Clerck, et
10 al. Detecting and tracking local changes in the tibiae of individual rats: a novel method to
11 analyse longitudinal in vivo micro-CT data. Bone. 2004;34(1):163-9.
- 12 75. Waarsing JH, JS Day, JAN Verhaar, AGH Ederveen, H Weinans. Bone loss dynamics
13 result in trabecular alignment in aging and ovariectomized rats. Journal of Orthopaedic
14 Research. 2006;24(5):926-35.
- 15 76. Stevenson JC, MS Marsh. An atlas of osteoporosis: CRC Press; 2007.
- 16 77. Alexopoulos LG, LA Setton, F Guilak. The biomechanical role of the chondrocyte
17 pericellular matrix in articular cartilage. Acta Biomaterialia. [doi:
18 10.1016/j.actbio.2005.02.001]. 2005;1(3):317-25.
- 19 78. Appelman TP, J Mizrahi, D Seliktar. A finite element model of cell-matrix
20 interactions to study the differential effect of scaffold composition on chondrogenic response
21 to mechanical stimulation. Journal of Biomechanical Engineering. 2011;133(4):041010.
- 22 79. Healy C, OD Kennedy, O Brennan, SM Rackard, FJ O'Brien, TC Lee. Structural
23 adaptation and intracortical bone turnover in an ovine model of osteoporosis. Journal of
24 Orthopaedic Research. 2010;28(2):248-51.
- 25 80. McNamara LM. Perspective on post-menopausal osteoporosis: establishing an
26 interdisciplinary understanding of the sequence of events from the molecular level to whole
27 bone fractures. Journal of The Royal Society Interface. 2010 March 6, 2010;7(44):353-72.
- 28 81. Martin R. Targeted bone remodeling involves BMU steering as well as activation.
29 Bone. 2007;40(6):1574-80.
- 30 82. Kalu DN, C-c Liu, RR HARDIN, BW HOLLIS. The aged rat model of ovarian
31 hormone deficiency bone loss. Endocrinology. 1989;124(1):7-16.
- 32 83. Štěpán J, J Pospichal, J Presl, V Pacovský. Bone loss and biochemical indices of bone
33 remodeling in surgically induced postmenopausal women. Bone. 1987;8(5):279-84.
- 34 84. Gallagher J. The pathogenesis of osteoporosis. Bone and Mineral. 1990;9(3):215-27.
- 35 85. Gallagher J, BL Riggs, J Eisman, A Hamstra, SB Arnaud, HF Deluca. Intestinal
36 calcium absorption and serum vitamin D metabolites in normal subjects and osteoporotic
37 patients: effect of age and dietary calcium. Journal of clinical investigation. 1979;64(3):729.
- 38 86. Heaney RP, R Recker, P Saville. Menopausal changes in calcium balance
39 performance. The Journal of laboratory and clinical medicine. 1978;92(6):953-63.
- 40 87. Reeve J, PJ Meunier, JA Parsons, M Bernat, O Bijvoet, P Courpron, et al. Anabolic
41 effect of human parathyroid hormone fragment on trabecular bone in involutional
42 osteoporosis: a multicentre trial. British medical journal. 1980;280(6228):1340.

- 1 88. Simkin A, J Ayalon, I Leichter. Increased trabecular bone density due to bone-loading
2 exercises in postmenopausal osteoporotic women. *Calcif Tissue Int.* 1987;40(2):59-63.
- 3 89. Wronski T, M Cintron, A Doherty, L Dann. Estrogen treatment prevents osteopenia
4 and depresses bone turnover in ovariectomized rats. *Endocrinology.* 1988;123(2):681-6.
- 5 90. Wronski T, L Dann, K Scott, L Crooke. Endocrine and pharmacological suppressors
6 of bone turnover protect against osteopenia in ovariectomized rats. *Endocrinology.*
7 1989;125(2):810-6.
- 8 91. Baron R, R Tross, A Vignery. Evidence of sequential remodeling in rat trabecular
9 bone: morphology, dynamic histomorphometry, and changes during skeletal maturation. *The*
10 *Anatomical Record.* 1984;208(1):137-45.

11

12